The University of Reading

The Assimilation of Satellite Derived Sea Surface Temperatures into a Diurnal Cycle Model

S. Pimentel[2], K. Haines[1] and N.K. Nichols[1]

NUMERICAL ANALYSIS REPORT 8/2007

[1]*School of Mathematics, Meteorology & Physics*
The University of Reading
Whiteknights, PO Box 220
Reading, RG6 6AX UK

[2]*Department of Earth Sciences*
Simon Fraser University
Burnaby
BC V5A 1S6 Canada

Department of Mathematics

The Assimilation of Satellite Derived Sea Surface Temperatures into a Diurnal Cycle Model

Sam Pimentel*, Keith Haines†, and Nancy K. Nichols‡

October 23, 2007

*Formally University of Reading now at Department of Earth Sciences, Simon Fraser University, Burnaby, British Columbia, V5A 1S6, Canada
sam_pimentel@sfu.ca
†Environmental Science Systems Centre, The University of Reading, UK
kh@mail.nerc-essc.ac.uk
‡Department of Mathematics, The University of Reading, UK
n.k.nichols@reading.ac.uk

Abstract

Satellite sea surface temperature (SST) observations available from infrared and microwave radiometers derive a skin and sub-skin temperature measurement from very near the ocean surface. These measurements, particularly those taken during the day under clear calm conditions, are often seen to have a diurnal warming signal. These diurnal SST signals can result in errors and aliasing when observations collected at different times of the day and from a variety of observation sources are merged together to obtain "foundation" or bulk SST observation products. A similar problem occurs when SST observations are assimilated into ocean models which typically do not resolve a diurnal cycle. In this paper a novel data assimilation method is developed and implemented that explicitly utilises diurnal signal information in SST observations. The technique assimilates SST observations taken over the day into a diurnal cycle model by making corrections, within uncertainty bounds, to the surface boundary forcing of the model. In particular, the surface wind speeds and the fractional cloud cover parameter, which are typically poorly known over the oceans, are tuned in the process. This method is shown to improve the estimate of diurnal SST variability and it has the potential to reduce uncertainties in estimates of foundation or bulk SST. As such the procedure can be viewed as a dynamic observation operator.

1 Introduction

Satellites measure SST either in the infrared (IR) or the microwave (MW) part of the electromagnetic spectrum. IR instruments derive a skin temperature and MW instruments the sub-skin temperature. Both these near surface observations can be

susceptible to diurnal warming signals [7]. Therefore the timing of the observations and the conditions in which the measurements are taken is very important. However, current ocean models are not able to resolve the near surface thermal micro-structure or adequately represent features of diurnal variability and therefore daytime SST observations are typically left out of model assimilation systems.

In the assimilation process the innovation vector $H(x) - y$ uses an observation operator H to transform model variables x onto an observed quantity y, so that a like-for-like comparison can be made. Typically x is the model temperature at the minimum depth, e.g. 5 m or deeper, in an ocean model that is run without diurnal forcing. This needs to be transformed in space and time to give a temperature at the near-surface, as measured by the satellite, which should have the diurnal signal represented when necessary. The observation operator clearly cannot be invariant as the transformation will depend on the particular local conditions at a given time. Developing such an operator is not an easy task; several attempts at parameterising the likely warming (e.g. [25], [10], [7], and [21]) have experienced difficulties in representing the full range of outcomes in this highly complex and non-linear system. A prognostic skin SST scheme has been tried with the ECMWF atmospheric model [26]; however, its effect on weather forecasting and four-dimensional data assimilation have yet to be fully examined.

In a previous paper [16] results are presented which show some degree of success in modelling the diurnal variability. This is achieved using a one-dimensional model called GOTM [24] which was modified specifically to improve diurnal cycle representation. This included improving near surface vertical resolution and incorporating state-of-the-art air-sea flux and ocean radiant heating parameterisations. The use of GOTM in this way can be viewed as providing a dynamic observation operator H, because by modelling the diurnal cycle and providing good near surface resolution we are able to quantify the transformation from a GCM's foundation temperature to skin or sub-skin temperature measured from space. However, the diurnal variability in GOTM relies on good forcing fields. The forcing error can be reduced by assimilating the observations directly into GOTM at the correct time and near-surface depth.

The extent of diurnal warming is predominately dependent on two key factors: sea surface wind speeds and the strength of the insolation, whose variance at a given location and time is largely determined by the cloud cover. As explained in [17] strong insolation during daytime, under clear skies, causes a warm stable stratified layer to appear, but this near surface warming can easily be broken down in the presence of wind driven mixing. The uncertainties in these forcing variables (cloud cover and wind speed) thus contribute to the uncertainty in the modelled diurnal warming estimates. Unfortunately in Numerical Weather Prediction (NWP) there is not a single, simple law which governs the formation of cloud and thus it is very difficult to parameterise and is a major source of uncertainty in model predictions. For example, Groisman et al [8] explicitly highlight cloud cover 'as one of the major trouble spots' of cloud parameterisation. Assumptions with respect to distributions of cloud cover throughout the atmosphere can significantly affect the energy budget [9].

Surface wind speeds over the oceans are also very difficult to assess in weather forecasting, particularly at low ($< 3\,\mathrm{ms}^{-1}$) and high ($> 20\,\mathrm{ms}^{-1}$) values where observa-

tional comparisons are difficult and errors vary for different regions and time scales [2]. In diurnal cycle modelling the high values are not of concern as no diurnal signal forms at high wind speeds; however, the diurnal warming is very sensitive to slight changes in wind speeds at the low values [22]. The wind speed, w, is important because wind stress increases roughly as $w^{2.7}$ and mixed layer deepening with w^4 [14]. Therefore even slight biases in NWP sea surface winds speeds can lead to systematic errors in ocean circulation models that are forced by these winds [2]. Wind speeds of less than $5\,\mathrm{ms}^{-1}$ account for nearly 40% of global hourly averaged winds [19]. Weak winds are concentrated in the tropics and sub- tropics where the majority of ocean to atmosphere heat flux occurs, and shifts in their patterns may affect the global heat budgets [19].

The aim of this paper is to use sea surface temperature (SST) observations over the day to provide additional information on the modelled upper layer temperatures. To bring the model projection closer to the observations, the forcing data during each day will need to be adjusted. Since the magnitude of any diurnal warming is primarily sensitive to wind speed and the cloud cover, the method developed here seeks to adjust forcing due to these factors, within feasible error bounds, in order to better fit the modelled SST to the observations recorded over each day. The modelled SST at observation depth, $\theta_{z^{\mathrm{obs}}}$, is represented as a non linear function of wind speed, w, and cloud cover, n,

$$\theta_{z^{\mathrm{obs}}} = \theta_{z^{\mathrm{obs}}}(w, n)\,. \tag{1}$$

The problem can then be stated as finding values of n and w such that

$$\left|\theta_{z^{\mathrm{obs}}} - \theta^{\mathrm{obs}}\right| \tag{2}$$

is minimised.

The paper proceeds as follows: in Section 2 an outline of the model and data used are given; this is then followed in Section 3 by a detailed description of the data assimilation method. In Section 4 results from employing this assimilation technique are presented, and finally conclusions are given in Section 5.

2 Model and Data

The model used in this study is that developed in a previous paper [16]. This is a one-dimensional mixed layer model, called GOTM that was optimised for the purposes of diurnal cycle modelling. The model is initialised with daily temperature and salinity profiles from the United Kingdom Meteorological Office (UKMO) 1° Forecasting Ocean Assimilation Model (FOAM) [1]. The mixed layer temperatures are then modified nightly by the UKMO Ocean Sea Temperature and Ice Analysis (OSTIA) product [20] which is representative of the foundation temperature and thus directly comparable to the surface of a GCM model such as FOAM. The FOAM-OSTIA innovation is applied throughout the diagnosed mixed layer depth to provide a more accurate night time temperature profile within the well mixed upper ocean. The model is then forced with six hourly meteorology from the European Centre for Medium-range Weather Forecasting (ECMWF).

Care is taken to convert the six hourly integrated solar flux from ECMWF to a finer time resolution that is critical for reproducing the diurnal cycle. This is achieved by integrating the Reed formula [18] over a six hour window, giving

$$\int_T^{T+6} I_0 dt = \int_T^{T+6} I_\downarrow \left(1 - 0.62n + 0.0019\beta\right)\left(1 - \alpha\right) dt, \tag{3}$$

where I_0 is the total surface solar radiation and $I_\downarrow$ is the surface insolation under clear skies, the fractional cloud cover value is denoted by n, albedo by α, β is the solar noon angle and T are the six hourly meteorological analysis times. The left hand side of Equation (3) is set equal to the integrated ECMWF flux value, and Equation (3) can then be rearranged to find an effective mean cloud parameter over this window,

$$n = \frac{\left(1 + 0.0019\beta\right)\int_T^{T+6} I_\downarrow(1-\alpha)dt - \int_T^{T+6} I_0 dt}{0.62\int_T^{T+6} I_\downarrow(1-\alpha)dt}. \tag{4}$$

If it is night, so that $\int_T^{T+6} I_\downarrow(1-\alpha)dt = 0$, then persistence $n_k = n_{k-1}$ (k denotes each 6hr analysis time) is assumed. A check is also made to enforce the physical cloud limits $0 \leq n \leq 1$. The net surface SWR, I_0, used in the model run is calculated at every time step using the Reed formula with the six hourly derived cloud values. Thus a much finer timescale is achieved, while the six hourly integrated ECMWF values are retained.

The penetration of the solar flux into the water column is calculated using the Ohlmann and Siegel parameterisation [13] and utilises SeaWiFS chlorophyll data. The air-sea fluxes are calculated using the TOGA-COARE algorithm [6] and [5]; this includes a cool-skin parameterisation [4]. The input data for this algorithm are the surface meteorology (air and dew point temperature, air pressure, and u and v wind speeds) together with the modelled SST.

Satellite derived SST observations are used both in the assimilation and to validate model output. These observations include a combination of infrared (SEVIRI) and microwave (AMSR-E and TMI) SSTs from the Global Ocean Data Assimilation Experiment (GODAE) High Resolution Sea Surface Temperature Pilot Project (GHRSST-PP), Level-2 Pre-processed (L2P) format data products. The data used for this study have the GHRSST estimated bias correction applied (a correction for long-term mean biases in the sensor) and have proximity confidence values labelled 'acceptable', 'excellent', and 'diurnal'. This choice selects observations uncontaminated by cloud (for infrared) or rain (for microwave), but retains observations that potentially have a diurnal signal. For more information on the data processing specifications adopted for the GHRSST products see [3]. The infrared retrieved SSTs are recognised as representing a skin SST and thus are compared to modelled temperatures which include a parameterised cool skin [4], whereas the microwave retrieved SSTs are representative of a temperature just below the cool skin effect and thus do not use this parameterisation.

3 Method

This section describes a method for tuning the cloud cover and the surface wind speed parameters, as they appear in the flux forcing algorithms for the GOTM model. It is assumed that these two parameters are likely to be the most poorly known from NWP or reanalysis model output. The parameters are used to help GOTM fit available satellite measurements including the diurnal cycle component.

3.1 The Algorithm

If we first consider the modelled SST, θ, as a function of the fractional cloud cover, n, and wind speed forcing, $w = \sqrt{u^2 + v^2}$,

$$\theta = \theta(n, w). \tag{5}$$

Parameters ϵ_A and ϵ_B are introduced where

$$n = n_b + \epsilon_A, \tag{6}$$

$$\begin{aligned} w &= (1 + \epsilon_B) w_b, & (7)\\ &= (1 + \epsilon_B)\sqrt{u_b^2 + v_b^2}. & (8) \end{aligned}$$

These adjustment parameters will be assumed to remain fixed over each 24 hour time window, although the background data: u_b, v_b, and n_b, from ECMWF change every six hours. The cloud correction is seen to be an absolute error, whereas the wind correction is a fractional error. This avoids corrections to wind direction and allows the strict limits on cloud cover, $0 \leq n \leq 1$, to be satisfied. The SST can now be viewed as a function of the parameters

$$\theta = \theta\left(\epsilon_A, \epsilon_B\right). \tag{9}$$

We now define a cost function $J = J\left(\epsilon_A, \epsilon_B\right)$ as;

$$J = \sum_{i=1}^{N} \left(H\left(\theta_i^{\text{model}}\right) - \theta_i^{\text{obs}} \right), \tag{10}$$

where N is the number of observations over the 24 hour window and H is an operator that picks the modelled sub-skin temperature for comparison with MW observations and the modelled skin temperature for IR observations. Notice that the cost function is not quadratic. If the initial $J_0 = J(0, 0) < 0$ then on average the SST observations are warmer than the model and therefore, to increase the size of the diurnal cycle, cloud cover and/or wind speeds need to be reduced (ϵ_A, $\epsilon_B < 0$). On the other hand if $J_0 > 0$ then the modelled SST is greater than the observations and the diurnal cycle needs to be reduced, which can be achieved by increasing cloud cover and/or wind speed (ϵ_A,

$\epsilon_B > 0$). The data assimilation problem can now be stated as follows;
An 'optimal' parameter pair $(\epsilon_A^*, \epsilon_B^*)$ *is sought such that for all feasible* (ϵ_A, ϵ_B)

$$|J(\epsilon_A^*, \epsilon_B^*)| \leq |J(\epsilon_A, \epsilon_B)| \,. \tag{11}$$

It is possible that an increase in cloud cover and a decrease in wind speeds and vice versa could provide the desired effect. In this scenario wind speed and cloud cover changes would partially cancel each other. However because the whole parameter space is not sampled and additional information, such as independent observations of cloud or wind, are not available, this possibility is excluded. The feasible parameter range for tuning is defined in two quadrants:

$$\begin{aligned} &0 < \epsilon_A \leq 1 - n_b, \\ &0 < \epsilon_B < 3, \end{aligned} \tag{12}$$

if $J_0 > 0$ and

$$\begin{aligned} &-n_b \leq \epsilon_A < 0, \\ &-1 < \epsilon_B < 0, \end{aligned} \tag{13}$$

if $J_0 < 0$.

The parameter tuning range is limited on physical grounds. The range for ϵ_A is limited by the maximum and minimum possible n throughout the 24 hour period. An upper bound on ϵ_B of 3 allows a 300% increase in the wind speed as an outside limit in cases of low wind speed. For higher background wind speeds the SST will not in any case be sensitive to variations in ϵ_B and thus for these situations the resulting large values of ϵ_B are excluded.

To solve this data assimilation problem we make the assumption that J varies linearly with respect to the parameters (ϵ_A, ϵ_B) within the feasible limits. A sequential process of optimising the parameters in turn is implemented. The ϵ_B parameter is found to be most sensitive and thus is tuned first. A control run followed by a run in which the ϵ_B parameter is perturbed is performed in order to gain a sensitivity estimate. This sensitivity estimate is then used to determine an 'optimal' parameter ϵ_B^*. This is then followed by a similar procedure for finding ϵ_A^*, and could be continued in a cycle by re-evaluating the optimal parameters in turn until convergence. However, in the interests of saving time this sequence is truncated after the first cycle. This method successfully manages to reduce J bringing it close to zero most of the time and a more sophisticated method is unlikely to yield better results. Further details of this procedure are provided in [15].

The SEVIRI observations are IR measurements and therefore are unable to penetrate through clouds. This additional information is used in the assimilation routine. The proximity confidence values chosen for this study suggest SEVIRI data are far from any clouds. Therefore if an IR observation is available the cloud cover value at this time is set to be zero, i.e. clear sky, and thereafter it is only the wind parameter that is tuned.

However, as IR radiometers are unable to view through cloud there are many occasions where IR SST observations are absent (roughly half the globe is thought to be covered by cloud at any one time [12]). Thus the assimilation algorithm also uses MW

observations (from AMSR-E and TMI). If both types (IR and MW) of observations are available then only the wind parameter is tuned, but if only MW observations are available then both wind and cloud parameters are tuned.

4 Assimilation Results

This assimilation algorithm was tested in an area of the south Atlantic, ($-45\,^{\circ}$N to $-25\,^{\circ}$N in latitude and $300\,^{\circ}$E to $330\,^{\circ}$E in longitude), known from modelled diurnal warming maps [16] to experience large diurnal variability. The experimental period was from 1st–7th January 2006, covering seven consecutive 24 hour assimilation cycles.

Where evaluating model-observation differences using IR measurements, the comparison is to the parameterised modelled skin temperature [4]. For the MW measurements the comparison is with the top modelled SST, at a depth of 0.015 m, without any cool skin effect. Statistical results are presented in Table 1, the total number of observations used in the comparisons are 6095. The control simulation makes no corrections to the forcing data. The cloud check runs reduce cloud cover to zero in the presence of IR observations. The wind correction performs the cloud check followed by an adjustment to the wind speeds at all observation locations. Finally, the wind then cloud correction runs makes an additional adjustment to cloud cover values (where there are MW observations only).

	Mean	STD	RMS
control	0.07	0.79	0.79
cloud check	0.06	0.78	0.78
wind correction	0.10	0.52	0.53
wind then cloud correction	0.07	0.49	0.49

Table 1: *Results showing the mean, STD, and RMS of* $\theta_{model} - \theta_{obs}$*, in* $^{\circ}C$ *for the area* $-45\,^{\circ}N$ *to* $-25\,^{\circ}N$ *and* $300\,^{\circ}E$ *to* $330\,^{\circ}E$ *during* 1^{st}–7^{th} *January 2006.*

The cloud check has only a very slight influence on the statistics; this may indicate that initial ECMWF cloud estimates were already zero, or low where IR observations are made, and therefore few corrections were necessary. If the SST observations are then used to adjust the wind forcing the standard deviation (STD) and root mean square (RMS) error are significantly reduced, with the RMS differences falling to $0.53\,^{\circ}$C. This is further reduced when a correction is made to cloud cover values on occasions when only MW observations are present. The resulting model-observation differences after assimilation may now be approaching the expected error accuracy of the observations (0.5 C) with the STD below those recorded in [23].

Figure 1 shows an example of the results of a wind then cloud correction assimilation run. It can be seen where GOTMs mixed layer temperatures are corrected nightly by OSTIA during the initialisation procedure. At this location no observations occurred during the first day (1st January 2006). During the last two days a diurnal signal is reasonably resolved by multiple satellite observations. The model control appears

to underestimate the warming on these occasions. However, earlier in the week the modelled diurnal warming estimates are larger than the observations suggest. The data assimilation method reduces the cloud, if necessary, in the presence of SEVIRI observations, followed by a correction to the wind speed forcing and then the cloud fractions (when SEVIRI observations are not present). The assimilation is able to reduce the modelled warming for days 2 through to 5, and increase the diurnal warming on days 6 and 7, thus fitting the observations much more closely. On days 2 and 5 the assimilation has not been able to reduce the warming as much as the observations would suggest. In these cases the system does not fully adhere to the assumptions of the assimilation routine either because the estimated sensitivity over the parameter range is inaccurate or the required change in forcing is outside the stated restrictions.

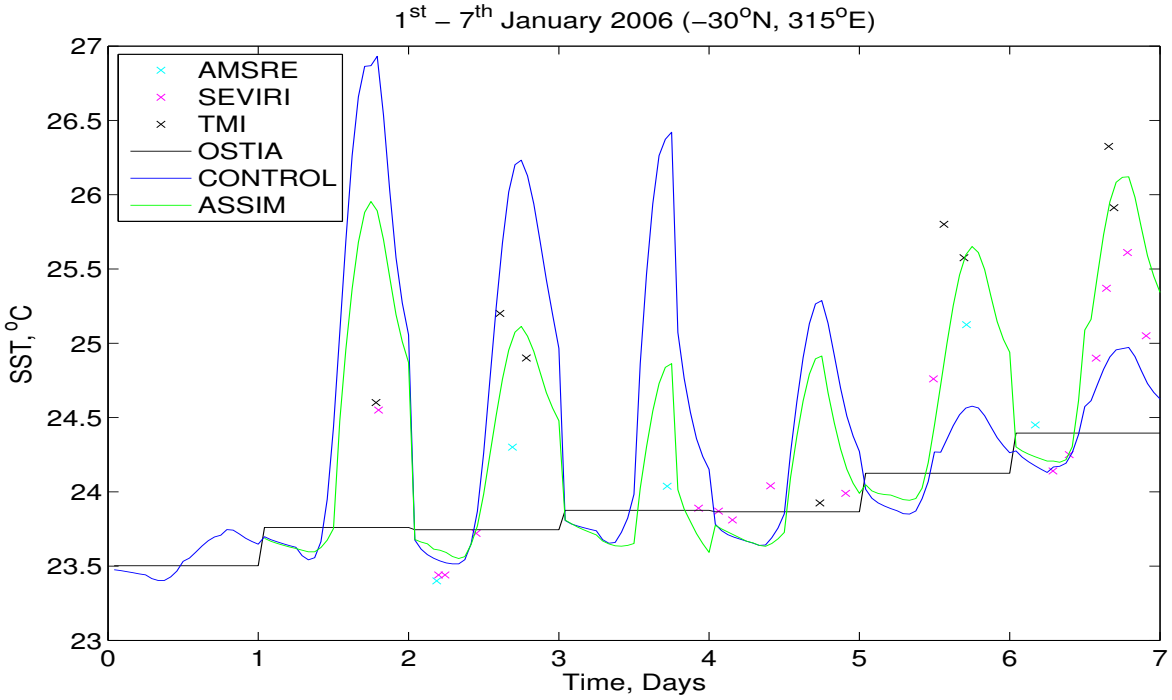

Figure 1: *A graph comparing the model SST before and after assimilation with the individual satellite observations and OSTIA at* $(-30\,°N,\ 315\,°E)$ *for the* 1^{st}–7^{th} *January 2006.*

In FIGURES 2 – 5 results from neighbouring locations are shown. The consistency of the changes in modelled SST induced by the assimilation at these nearby locations suggest that the SST corrections are sensible. The changes produced by the assimilation run are calculated independently at each location. In Figure 2 (−29 °N, 315 °E) the results are almost identical except the warming on day 3 is not reduced as much as previously. Further south in Figure 3 (−29 °N, 315 °E) only one observation is present on day 2 and this causes a larger diurnal cycle, against the trend at nearby locations. On day 7 at (−29 °N, 315 °E) and Fig 5 (−30 °N, 314 °E) the observations suggest the diurnal warming is close to that estimated by the control, unlike the other locations where the control is deemed an under estimation. At (−30 °N, 314 °E) in Figure 5 on

day 5 OSTIA shows a warm bias compared to the observations and this is likely the cause of the assimilation run to fail at this point.

The assimilation is less robust if a correction to the diurnal cycle is based on a single observation, particularly if it occurs early in the morning. This can be seen in Figure 3 where on day 2 a slight correction early in the warming phase leads to a larger diurnal cycle that can not be attested by further observations and on day 4 where as a result of a possible erroneously cool observation strong winds are used to eliminate any diurnal cycle. These examples illustrate how the scheme could be further improved in the future by incorporating more observations and building on the knowledge gained to form a careful treatment of observational error, both systematic and random, within the assimilation cycle.

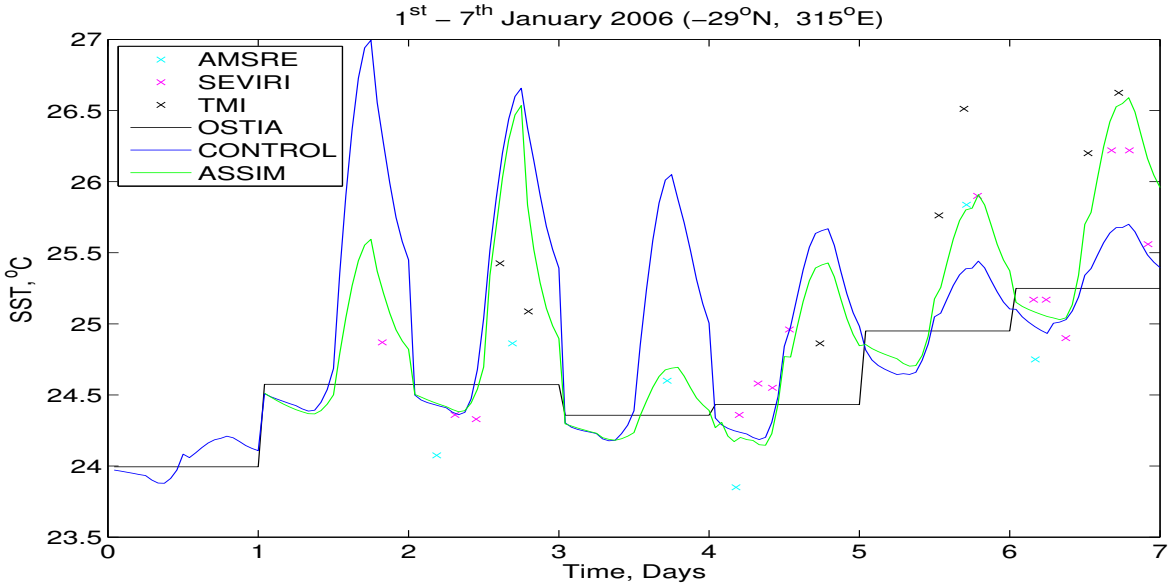

Figure 2: *A graph comparing the model SST before and after assimilation with the individual satellite observations and OSTIA at* $(-29\,^{\circ}N,\ 315\,^{\circ}E)$ *for the* 1^{st}–7^{th} *January 2006.*

4.1 Spatial Patterns

The estimates of the diurnal warming of SSTs can also be viewed spatially over the whole area. These results are shown in Figure 6 where the magnitude of the diurnal warming is defined as the difference between the maximum and minimum temperature over the day at the shallowest modelled depth of 1.5 cm. A diurnal warming signal of zero is given if the SST at the start is also the maximum/minimum over the day; this eliminates the misinterpretation of any cooling/warming trend. In Figure 6 the plots in the left column show the diurnal warming before assimilation and the plots in the middle and right columns are the diurnal warming maps after assimilation. The assimilation only works at locations where observations are present and these are shown in the centre column. The progress down the column displays how the

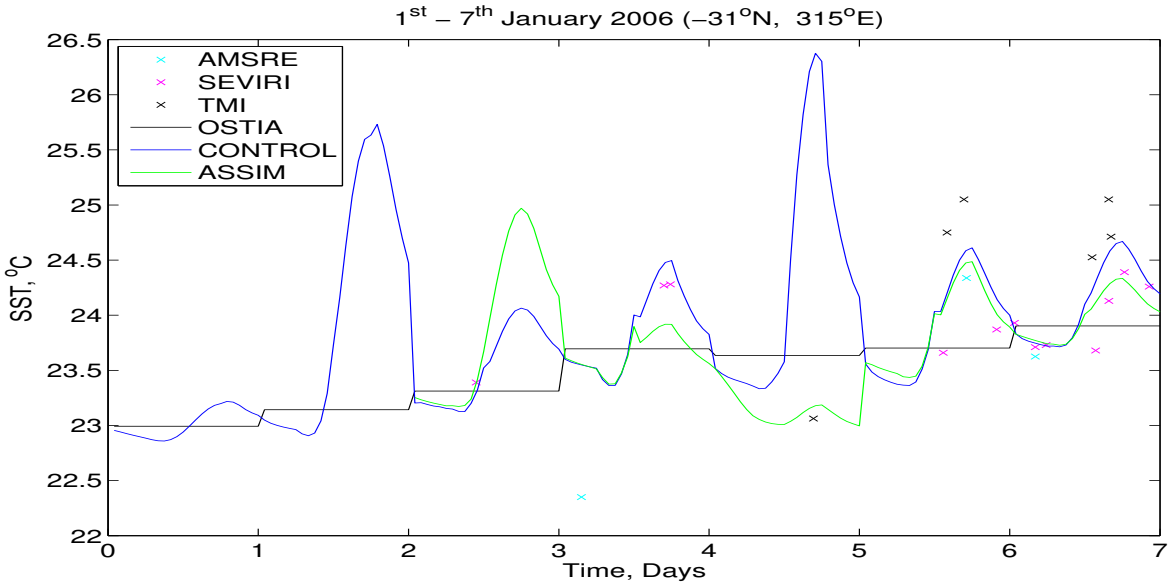

Figure 3: *A graph comparing the model SST before and after assimilation with the individual satellite observations and OSTIA at* $(-31\,^{\circ}N,\ 315\,^{\circ}E)$ *for the* 1^{st}–7^{th} *January 2006.*

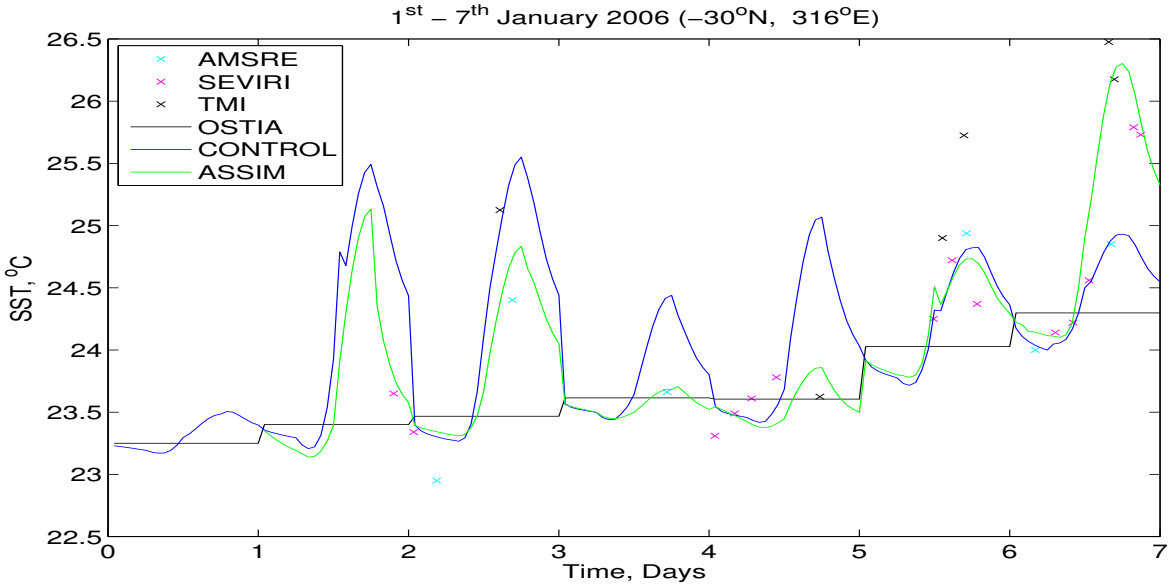

Figure 4: *A graph comparing the model SST before and after assimilation with the individual satellite observations and OSTIA at* $(-30\,^{\circ}N,\ 316\,^{\circ}E)$ *for the* 1^{st}–7^{th} *January 2006.*

diurnal warming pattern evolves over time, day by day. The white triangle in the top left hand corner is the coast of South America and the white patches in the centre column are areas where no satellite observations were available, and on these occasions

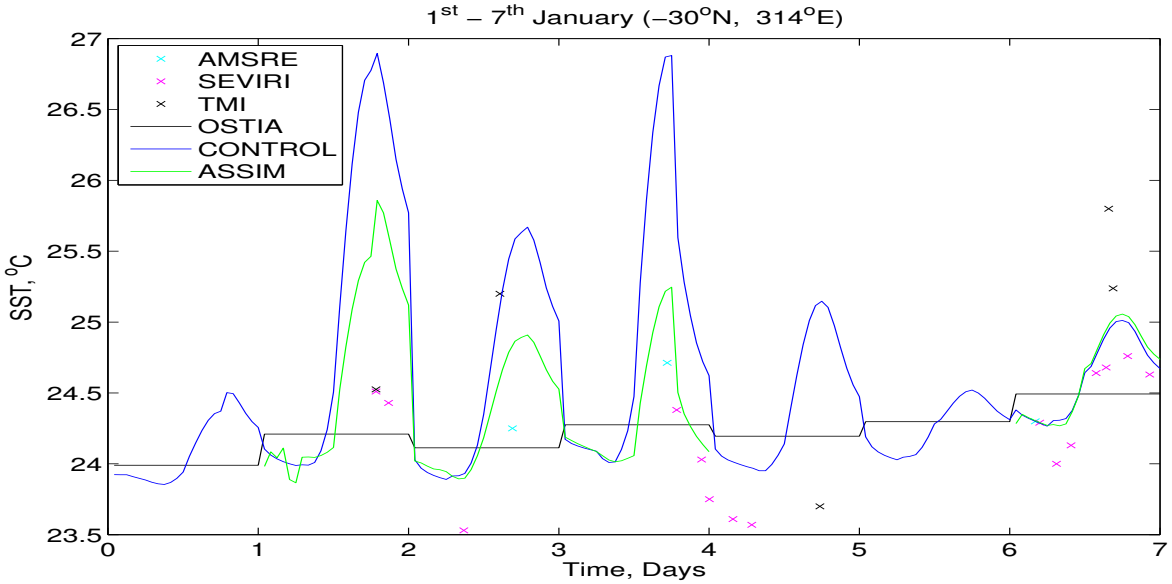

Figure 5: *A graph comparing the model SST before and after assimilation with the individual satellite observations and OSTIA at* $(-30\,^{\circ}N,\ 314\,^{\circ}E)$ *for the* 1^{st}–7^{th} *January 2006.*

the initial model estimates remained unchanged.. Generally speaking the assimilation seems to have slightly weakened the diurnal signal in areas of very strong modelled diurnal warming. Areas where the assimilation has increased warming can also be seen, particularly on the 6th and 7th of January 2006. The patch of warming occurring on the 6th January 2006 appears less intense and more spread out after the assimilation. On the 7th January the modelled estimates before assimilation show two separate patches of strong diurnal warming. After assimilation the warming in the north-eastern corner again appears less intense and is spread towards the coast. The other patch of strong warming has moved further to the south-west.

The changes to the forcing can be viewed in FIGURES 7 and 8. The daily averaged wind stress is changed by adjustments to the wind speeds in the assimilation and the daily peak SWR will be affected by adjustments to cloud cover in the assimilation. What is immediately noticeable is the rather noisier fields after assimilation. This is in part a consequence of the scattered distribution of available observations in space and time and of using independent 1-D models to calculate adjustments, while the initial fields are provided from a global 3-D atmospheric model. These adjustments or corrections could be smoothed horizontally and the information spread from areas high in observations to areas with low observation densities. However, the corrections have an association with fine scale, non-linear wind structure and patchy cloud cover to which the diurnal variability can be extremely sensitive, and thus smoothing would not necessarily be appropriate.

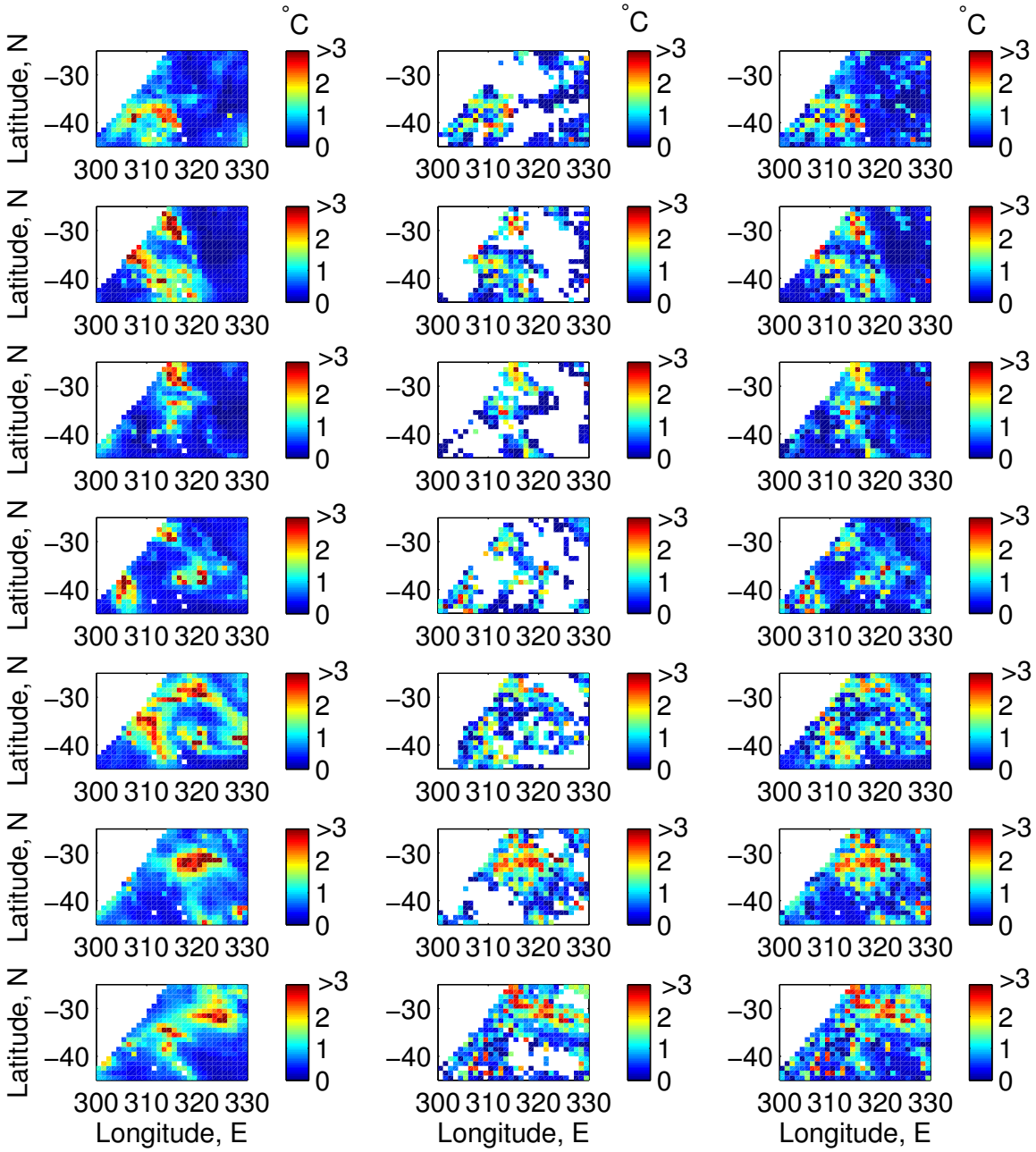

Figure 6: *The maps in the left column show modelled diurnal warming estimates before data assimilation and the those in the middle and right columns are the diurnal warming estimates after assimilation, with the graphs in the middle column only showing values where satellite SST observations were available. The graphs down the columns represent successive days from* 1^{st} *to the* 7^{th} *January 2006.*

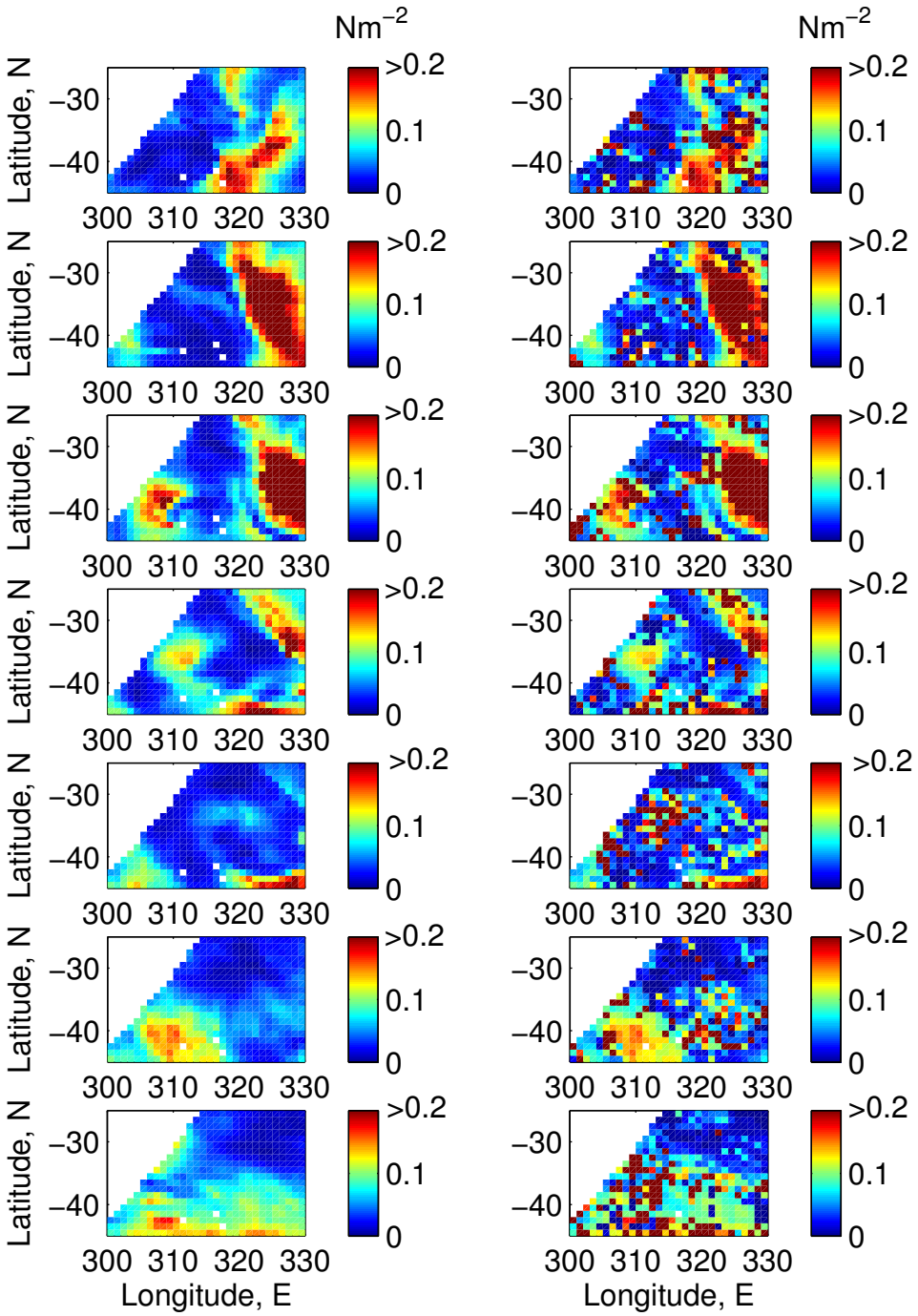

Figure 7: *The maps in the left column show the daily mean wind stress before data assimilation and the those in the right column are after assimilation (values in* Nm^{-2}*). The graphs down the columns represent successive days from* 1^{st} *to the* 7^{th} *January 2006.*

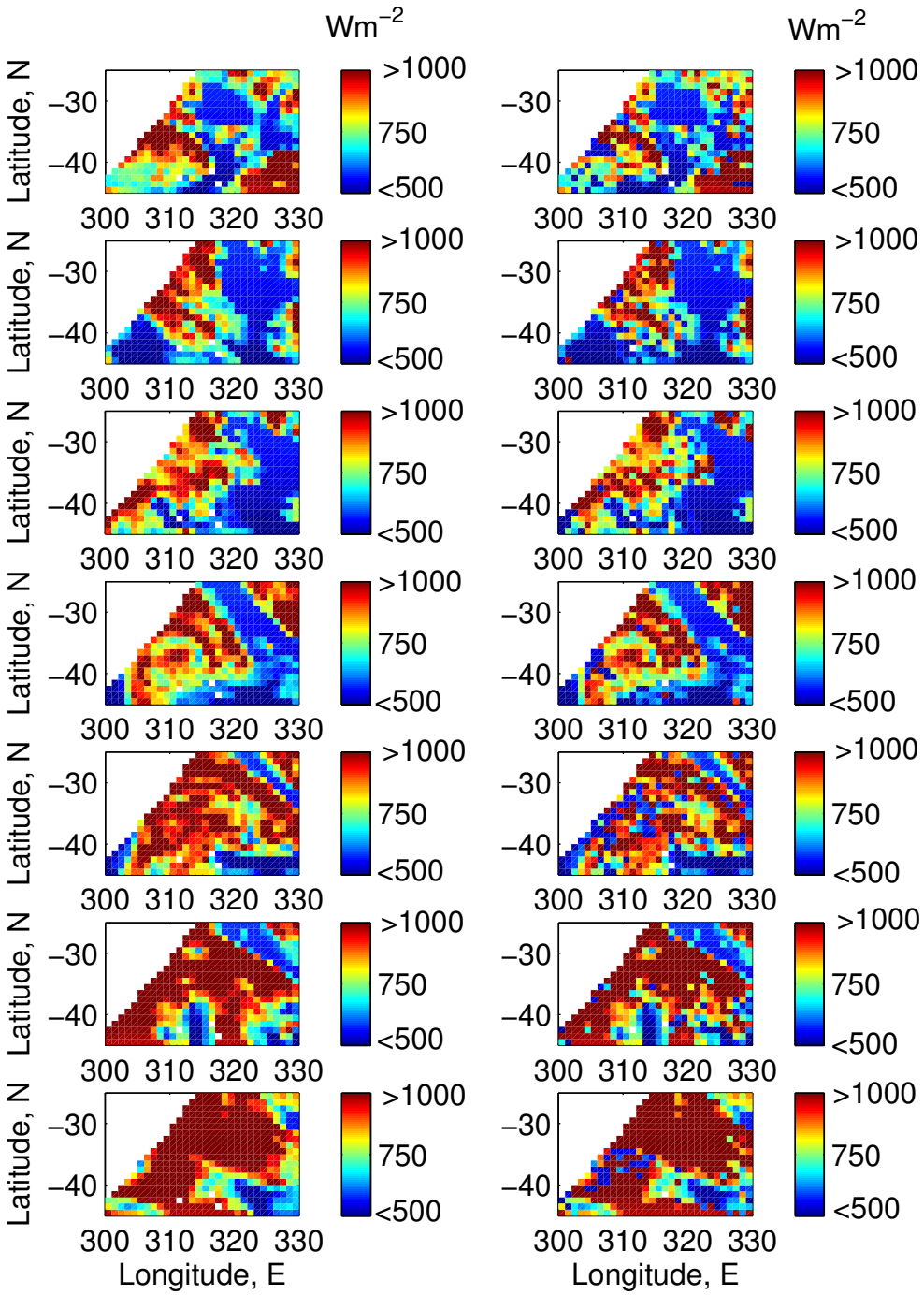

Figure 8: *The maps in the left column show daily peak SWR before data assimilation and the those in the right column are after assimilation (values in* Wm^{-2}*). The graphs down the columns represent successive days from* 1^{st} *to the* 7^{th} *January 2006.*

4.2 Comparing Different Satellite Observations

Further analyses were also performed to assess the errors associated with individual observation types relative to the control run and these are presented in Table 2.

	No. Obs.	Mean	STD	RMS
GOTM-SEVIRI	2343	−0.25	0.57	0.62
GOTM-AMSRE	2220	0.20	0.77	0.80
GOTM-TMI	1532	0.37	0.91	0.98

Table 2: *Results showing the number of observations, the mean, STD, and RMS of* $\theta_{control} - \theta_{obs}$*, in* $^\circ C$*, for individual satellite types for the area* $-45\,^\circ N$ *to* $-25\,^\circ N$ *and* $300\,^\circ E$ *to* $330\,^\circ E$ *during* 1^{st}–7^{th} *January 2006.*

A similar number of SEVIRI and AMSRE observations are available over the time period in this area, with slightly fewer TMI observations. The model-observation match-ups reveal differences between the three satellite instruments. The SEVIRI observations are shown to be on average warmer than the parameterised skin temperature. Whereas the AMSRE and TMI observations are cooler on average than the modelled SST. This suggests that the observations have some systematic errors in this area at this time, with SEVIRI SST systematically too warm and/or AMSRE and TMI observations systematically too cool. The model could also have a warm bias and be estimating too great a cool skin correction. This seems unlikely as the parameterised cool skin correction for this period was on average 0.15 °C, i.e. smaller than the SEVIRI only mean difference. The model simulations are dependent on the OSTIA SST at the start of each day; therefore any errors in OSTIA will also be apparent (see Section 4.4). The STD and RMS are significantly lower when comparing SEVIRI observations with either AMSRE or TMI. The largest errors are found with the TMI observations, where the RMS error approaches 1 °C.

4.3 Day-Night Comparisons

Differences in night time (between the restricted hours of 22:00–04:00 local time) and daytime (between the hours 10:00–16:00 local time) match-ups were also compared. The total number of observation comparisons were 3243 during the daytime hours and 1488 during the night time hours. The model was initialised to OSTIA between the stated night time hours. The results shown in Table 3 indicate much larger mean differences during daytime. It looks likely that on average the model is over estimating the diurnal warming signal by exaggerating the daytime warming and night time cooling. An alternative explanation could be that the retrieval algorithms, which are empirically tuned against buoy observations (these buoy measurements record a temperature at a deeper depth, typically around a metre), have inadvertently suppressed the true warming signal. However, by comparing the results before and after assimilation in Table 3 it can be seen that the assimilation is very effective at reducing the tendency

for a heighten diurnal cycle and draws the model closer to the observations. The STD and RMS differences remain similar for both day and night.

	Mean	STD	RMS
Before Assimilation			
daytime	0.29	0.88	0.93
night time	-0.15	0.57	0.59
After Assimilation			
daytime	0.14	0.51	0.53
night time	0.00	0.50	0.50

Table 3: *Results showing the mean, STD, and RMS of* $\theta_{model} - \theta_{obs}$*, before and after the assimilation, in* $^\circ C$*, during daytime (10–16) and night time (22–04) local time for the area* $-45\,^\circ N$ *to* $-25\,^\circ N$ *and* $300\,^\circ E$ *to* $330\,^\circ E$ *during* 1^{st}–7^{th} *January 2006.*

4.4 Comparisons to OSTIA

To help determine to what extent the biases are due to model or observations the individual satellite observations were also compared to the OSTIA values. The results of the mean, STD, and RMS of OSTIA minus the observations are presented in Table 4.

	Mean	STD	RMS
SEVIRI only	−0.22	0.51	0.56
AMSRE only	−0.08	0.69	0.70
TMI only	−0.20	0.84	0.87
all obs	−0.17	0.67	0.69
daytime SEVIRI only	−0.51	0.56	0.76
daytime AMSRE only	−0.29	0.71	0.77
daytime TMI only	−0.22	0.86	0.89
daytime all obs	−0.31	0.76	0.82
night time SEVIRI only	0.06	0.37	0.38
night time AMSRE only	0.19	0.56	0.59
night time TMI only	–	–	–
night time all obs	0.14	0.51	0.53

Table 4: *Results showing the mean, STD, and RMS of* $\theta_{OSTIA} - \theta_{obs}$*, in* $^\circ C$*, including daytime (10–16) and night time (22–04) local time for the area* $-45\,^\circ N$ *to* $-25\,^\circ N$ *and* $300\,^\circ E$ *to* $330\,^\circ E$ *during* 1^{st}–7^{th} *January 2006.*

The results shown in Table 4 reveal that SEVIRI has the largest bias but smallest RMS difference of the three instruments when compared to OSTIA. The biases are all negative for daytime observations and all positive for night time observations. Note that no night time TMI observations occurred during this period. The daytime biases

are found to be larger than night time biases and when comparing all observations, a bias of $-0.17\,^{\circ}\mathrm{C}$ is found. This indicates that the satellite observations on average are warmer than OSTIA, as would be expected because OSTIA is largely restricted to night-time. The sharp difference in day and night time mean values demonstrates the presence of diurnal signals in the daytime observations. OSTIA is the mean value of these observations, as well as others, and so the expectation is that the bias would be small. In this match-up all observations are included whereas OSTIA is formed by eliminating daytime observations taken with wind speeds less than $6\,\mathrm{ms}^{-1}$. These additional observations are therefore contributing to the slight cool bias in OSTIA. Comparing results in Tables 4, 3, and 1 indicates that the modelled control simulation has a smaller mean error than OSTIA, but produces slightly larger STD and RMS errors than OSTIA. However, after data assimilation of the L2P satellite data, the analysis is a much better representation of the observed SSTs, with reduced mean, RMS, and STD. For example, the persistence assumption of OSTIA reveals an overall mean error of $-0.17\,^{\circ}\mathrm{C}$, a STD of $0.67\,^{\circ}\mathrm{C}$, and an RMS error of $0.69\,^{\circ}\mathrm{C}$, whereas assimilating observations into the diurnal cycle model reduced the overall mean error to $0.07\,^{\circ}\mathrm{C}$ and the STD and RMS error to $0.49\,^{\circ}\mathrm{C}$. This is an improvement of 59% in the mean error, 27% in the STD, and 29% in the RMS error.

4.5 Using Satellite Wind Measurements

The AMSRE and TMI instruments also measure wind speeds and these data are provided with the GHRSST-PP L2P products. These observations when available may provide an improvement on the ECMWF forecast winds. Therefore model simulations were performed in which the instantaneous satellite wind speeds were used whenever they were available to adjust the six hourly ECMWF wind values. The model requires the wind components u and v thus the ECMWF values were adjusted by a factor, γ, such that $w_{sat} = \sqrt{\gamma u^2 + \gamma v^2}$, where w_{sat} is calculated as the mean value of satellite wind observations occurring during the six hourly window. However, this model (control) simulation resulted in a worse mean model-observations SST difference of $0.17\,^{\circ}\mathrm{C}$ and a similar RMS difference of $0.78\,^{\circ}\mathrm{C}$ when compared to results using ECMWF winds only (see control in Table 1).

The availability of these satellite wind measurements also allows for a comparison to be made between the original ECMWF wind values and the corrected wind values after the assimilation. These results are presented in Table 5.

The results in Table 5 reveal that the satellite measured winds, particularly from TMI, are slightly stronger than those forecast by ECMWF. The RMS differences between the ECMWF winds and all the satellite derived winds is $1.73\,\mathrm{ms}^{-1}$. After the ECMWF winds have been corrected in the assimilation process the RMS is approximately increased by $1\,\mathrm{ms}^{-1}$ in all cases. However, the resulting error is just outside the quoted mission accuracy of the AMSRE product ($1\,\mathrm{ms}^{-1}$) [11], although validation against buoy and scatterometer data at very low wind speeds is particularly difficult [11]. This suggests further work maybe required before the potential of having concurrent observations of SST and wind speed can be fully utilized in aiding our understanding of the diurnal cycle.

	No. Obs.	Mean	RMS	STD
ECMWF-AMSRE	2009 (1635)	−0.07 (−0.12)	1.76 (1.72)	1.76 (1.71)
ASSIM-AMSRE	1635	−0.23	2.74	2.73
ECMWF-TMI	1278 (1212)	−0.49 (−0.49)	1.68 (1.60)	1.61 (1.52)
ASSIM-TMI	1212	−0.45	2.57	2.53
ECMWF-ALL	3287 (2847)	−0.23 (−0.28)	1.73 (1.67)	1.71 (1.64)
assim-ALL	2847	−0.33	2.67	2.65

Table 5: *Results comparing the ECMWF forecast wind speeds before and after assimilation to the AMSRE and TMI wind measurements showing the number of observations, the mean, the RMS, and STD differences in* ms^{-2}*. For the area* $-45\,^{\circ}N$ *to* $-25\,^{\circ}N$ *and* $300\,^{\circ}E$ *to* $330\,^{\circ}E$ *during* 1^{st}–7^{th} *January 2006. The numbers in parenthesis are calculations only at the locations and times when wind speeds are corrected in the assimilation.*

5 Conclusion

In this paper a data assimilation method has been developed that assimilates satellite derived SST observations into a diurnal cycle model. It is proposed how model errors in diurnal warming estimates are primarily caused by uncertainties in NWP forcing data. The diurnal variability of SSTs can be viewed as a function of wind speeds and fractional cloud cover. Observations from SEVIRI, AMSRE, and TMI occurring throughout the day are compared to their modelled equivalent. The resulting differences are then reduced by making corrections to the forcing wind speeds and cloud cover. This tuning of the forcing is shown to result in modelled SST estimates that resemble available observations much more closely. The assimilation method could be viewed as smoothing and interpolating the satellite SST observations in an intelligent manner. The method is shown, for example, to fit the observations better than OSTIA, which uses a daily persistence assumption.

Most SST assimilation schemes do not use vertical correlation scales when inserting SST observations and subsequently are unable to provide adjustments to the subsurface thermodynamic structure; this reduces the effectiveness of an assimilation. However, by correcting wind speed and cloud cover values, within uncertainty bounds, the method presented here attempts to preserve the balance of thermal and dynamical fields within the diurnal thermocline.

This assimilation method could be implemented on a much wider scale to build up a detailed real time picture of diurnal warming across the world's oceans. The distribution and magnitude of diurnal signals are still relatively unknown and this technique of merging observations with a diurnal cycle model could be used to improve this situation. Another application could be to use this technique to calculate foundation temperatures of increased accuracy. For example, the method could be used to re-calculate the OSTIA product. This could be achieved by assimilating all of the observations (i.e. including daytime observations recorded in low wind speeds) into the diurnal cycle model in order to accurately calculate the foundation temperature. In

using a model with the fine scale temporal and near surface spatial resolution we would be able to identify the temperature from which the diurnal cycle develops. It is also shown how there is scope to improve on the techniques developed here; by improving our understanding of errors associated with the different satellite data types and model estimates.

References

[1] M. J. Bell, R. M. Forbes, and A. Hines. Assessment of the FOAM global data assimilation system for reat-time operational ocean forecasting. *J. Mar. Syst.*, 25:1–22, 2000.

[2] D. B. Chelton and M. H. Freilich. Scatterometer-based assessment of 10-m wind analyses from the operational ECMWF and NCEP numerical weather prediction models. *Mon. Wea. Rev.*, 133:409–429, 2005.

[3] C. J. Donlon and the GHRSST-PP Science Team. The recommended GHRSST-PP data processing specifications GDS (version 1 revision 1.5). Technical Report 17, GHRSST-PP, 2004.

[4] C. W. Fairall, E. F. Bradley, J. S. Godfrey, G. A. Wick, J. B. Edson, and G. S. Young. Cool-skin and warm-layer effects on sea surface temperature. *J. Geophys. Res.*, 101:1295–1308, 1996.

[5] C. W. Fairall, E. F. Bradley, J. E. Hare, A. A. Grachev, and J. B. Edson. Bulk parameterization of air-sea fluxes: Updates and verification for the COARE algorithm. *J. Climate*, 16:571–591, 2003.

[6] C. W. Fairall, E. F. Bradley, D. P. Rogers, J. B. Edson, and G. S. Young. Bulk parameterization of air-sea fluxes for TOGA-COARE. *J. Geophys. Res.*, 101:3747–3764, 1996.

[7] C. L. Gentemann, C. J. Donlon, A. Stuart-Menteth, and F. J. Wentz. Diurnal signal in satellite sea surface temperature measurements. *Geophys. Res. Lett.*, 30:1140, 2003.

[8] P. Y. Groisman, R. S. Bradley, and B. Sun. The relationship of cloud cover to near-surface temperature and humidity: comparison of GCM simulations with empirical data. *J. Climate*, 13:1858–1878, 2000.

[9] C. Jakob and S. Klein. The role of vertically varying cloud fraction in the parametrization of microphysical processes in the ECMWF model. *Q. R. Meteorol. Soc.*, 125:941–965, 1999.

[10] Y. Kawai and H. Kawamura. Evaluation of the diurnal warming of sea surface temperature using satellite-derived marine meteorological data. *J. Oceanogr.*, 58:805–814, 2002.

[11] S. Martin. *An introduction to ocean remote sensing*. Cambridge Univerisity Press, 2004.

[12] R. McIlveen. *Fundamentals of Weather and Climate*. Chapman and Hall, London, second edition, 1992.

[13] J. C. Ohlmann and D. A. Siegel. Ocean radiant heating. Part II: Parameterizing solar radiation transmission through the upper ocean. *J. Phys. Oceanogr.*, 30:1849–1865, 2000.

[14] Working Group on Air-Sea Fluxes (WGASF). Intercomparison and validation of ocean-atmosphere energy flux fields, final report of the joint WCRP/SCOR working group on air-sea fluxes (SCOR working group 110). Technical report, World Climate Research Programme, 2000.

[15] S. Pimentel. *Estimation of the Diurnal Variability of Sea Surface Temperatures using Numerical Modelling and the Assimilation of Satellite Observations*. PhD thesis, University of Reading, 2007.

[16] S. Pimentel, K. Haines, and N. K. Nichols. Modelling the diurnal variability of sea surface temperatures. University of Reading, Department of Mathematics, Numerical Analysis Report 7/2007 (submitted for publication).

[17] J. F. Price and R. A. Weller. Diurnal cycling: Observations and models of the upper ocean response to diurnal heating. *J. Geophys. Res.*, 91, 1986.

[18] R. K. Reed. On estimating insolation over the ocean. *J. Phys. Oceanogr.*, 7:482–485, 1977.

[19] K. Shankaranarayanan and M. A. Donelan. A probabilistic approach to scatterometer function verification. *J. Geophys. Res.*, 106:19969–19990, 2001.

[20] J. Stark and C. Donlon. A new high-resolution operational sea surface temperature analysis for oceanography and meteorology. *Eos Trans. AGU, Ocean Sci. Meet. Suppl.*, 87:Abstract OS12A–04, 2006.

[21] A. C. Stuart-Menteth, I. S. Robinson, and C. J. Donlon. Sensitivity of the diurnal warm layer to meteorological fluctuations. Part 2: A new parameterisation for diurnal warming. *Journal of Atmospheric and Ocean Science*, 10:209–234, 2005.

[22] A. C. Stuart-Menteth, I. S. Robinson, R. A. Weller, and C. J. Donlon. Sensitivity of the diurnal warm layer to meteorological fluctuations. Part 1: Observations. *Journal of Atmospheric and Ocean Science*, 10:193–208, 2005.

[23] Remote Sensing Systems. http://www.remss.com, April 2007.

[24] L. Umlauf, H. Burchard, and K. Bolding. *General Ocean Turbulence Model. Scientific documentation. v3.2*. Marine Science Reports no. 63, Baltic Sea Research Institute Warnemnde, Warnemnde, Germany, 2005.

[25] P. J. Webster, C. A. Clayson, and J. A. Curry. Clouds, radiation, and the diurnal cycle of sea surface temperature in the tropical western Pacific. *J. Climate*, 9:1712–1730, 1996.

[26] X. Zeng and A. Beljaars. A prognostic scheme of sea surface skin temperature for modelling and data assimilation. *Geophys. Res. Lett.*, 32:14605–14609, 2005.